Available online at www.sciencedirect.com

SciVerse ScienceDirect

Nuclear Physics A 872 (2011) 196–209

NUCLEAR PHYSICS A

www.elsevier.com/locate/nuclphysa

# Heavy quark production at LHC in the color dipole formalism

E.R. Cazaroto [a], V.P. Gonçalves [b], F.S. Navarra [a,*]

[a] *Instituto de Física, Universidade de São Paulo, C.P. 66318, 05315-970 São Paulo, SP, Brazil*
[b] *Instituto de Física e Matemática, Universidade Federal de Pelotas, Caixa Postal 354, CEP 96010-900, Pelotas, RS, Brazil*

Received 16 August 2011; received in revised form 22 September 2011; accepted 28 September 2011

Available online 6 October 2011

**Abstract**

In this work we estimate the heavy quark production in proton–proton and proton–nucleus collisions at LHC energies using the color dipole formalism and the solution of the running coupling Balitsky–Kovchegov equation. Nuclear effects are considered in the computation of the total cross sections and rapidity distributions for scattering on protons and nuclei.


*Keywords:* Heavy quark production; High energy collisions; Color glass condensate

## 1. Introduction

Heavy quark production in high energy collisions is important for a number of reasons. One of them is that it offers a good testing ground for perturbative QCD (pQCD) calculations, which in spite of the continuous progress over the last thirty years, still contain some ambiguities, mostly related to scale dependence of the observable quantities. In the context of pQCD there are different calculation schemes. The most well known is the collinear factorization approach, which has been developed up to Next-to-Leading Order (NLO) in $\alpha_s$ [1–4]. More recently the Fixed Order plus Next-to-Leading-Log (FONLL) [5] was developed. It resumes large perturbative terms proportional to powers of $\alpha_s \log(p_T/m_Q)$ where $p_T$ and $m_Q$ are the heavy quark transverse momentum and mass, respectively. In these calculations all particles involved are assumed to

* Corresponding author.
*E-mail address:* navarra@if.usp.br (F.S. Navarra).

0375-9474/$ – see front matter 
doi:10.1016/j.nuclphysa.2011.09.017

be on mass shell, carrying only longitudinal momenta, and the cross section is averaged over two transverse polarizations of the incident gluons. The virtualities $Q^2$ of the initial partons are taken into account only through their structure functions. The formalism which incorporates the incident parton transverse momenta is referred to as the $k_T$-factorization approach [6–14]. In this approach the Feynman diagrams are calculated taking into account the virtualities and all possible polarizations of the incident partons. In the $k_T$-factorization approach the unintegrated gluon distributions are used instead of the usual structure functions.

In proton nucleus collisions the linear $A$-dependence of the heavy flavor production cross sections is usually assumed, so the obtained results are discussed in terms of the cross section scaled to $pp$ collision. In perturbative QCD with the factorization approximation, heavy ion collisions differ from $pp$ collisions only by the change of the usual nucleon structure functions or unintegrated gluon distributions by the same functions for bound nucleons. At RHIC energies the difference between bound and unbound parton structure functions is known from EMC and NMC experimental data and their DGLAP evolution analysis. From these studies we have learned that nuclear effects in charm production at RHIC cause a deviation of 5–10% from the linear ($A$-dependent) predictions. The experimental data of the PHENIX [15,16] Collaboration obtained at RHIC both from pp and nuclear collisions are in reasonable agreement with the NLO QCD and with the $k_T$ factorization approach predictions. The existing STAR [17] Collaboration data are in contradiction with the PHENIX data and with standard QCD calculations. However a reanalysis of these data is in progress.

Calculations performed with other approaches, also based on pQCD, are welcome and may be very useful to cross-check and complement previous analyses. In this paper we calculate heavy quark production cross sections using a formalism derived from the high energy regime of QCD (for recent reviews see Ref. [18]). In this regime, perturbative QCD predicts that the small-$x$ gluons in a hadron wave function should form a Color Glass Condensate (CGC), which is characterized by the limitation on the maximum phase-space parton density that can be reached in the hadron wave function (parton saturation), with the transition being specified by a typical scale, which is energy dependent and is called saturation scale $Q_{\rm sat}$. In order to estimate the saturation effects we study heavy quark production using the color dipole approach, which gives a simple and unified picture of this process in photon–hadron and hadron–hadron interactions (for related studies see Refs. [19–25]). It is important to emphasize that in contrast to the heavy quark production in the previous accelerators (SPS, Tevatron and RHIC), where the saturation scale $Q_{\rm sat}$ is smaller than the typical hard scale, $\mu = m_Q$, at the LHC energies, we probe for the first time the kinematical regime where $Q_{\rm sat} \approx \mu$. Therefore, at these energies one may expect a sizeable modification of the heavy quark total cross sections and rapidity distributions.

This paper is organized as follows. In next section (Section 2) we present a brief review of the heavy quark production in the color dipole formalism, introducing the main formulae. In Section 3 we discuss the QCD dynamics and the models used in the calculations. In Section 4 we present our predictions for the total cross sections and rapidity distributions for heavy quark production in $pp$ and $pA$ collisions. Finally, in Section 5 we summarize our main results and conclusions.

## 2. Heavy quark production in the color dipole formalism

Heavy quark hadroproduction at high energies has been usually described considering the collinear factorization, where all partons involved are assumed to be on mass shell, carrying only longitudinal momenta, and their transverse momenta are neglected in the QCD matrix elements.

The cross sections of the QCD subprocess are usually calculated in leading order (LO), as well as in next-to-leading order (NLO). In particular, the cross sections involving incoming hadrons are given, at all orders, by the convolution of intrinsically non-perturbative (but universal) quantities – the parton densities – with perturbatively calculable hard matrix elements, which are process dependent. The conventional gluon distribution $G(x, \mu^2)$, which drives the behavior of the observables at high energies, corresponds to the density of gluons in the proton having a longitudinal momentum fraction $x$ at the factorization scale $\mu$. This distribution satisfies the DGLAP evolution in $\mu^2$ and does not contain information about the transverse momentum $k_T$ of the gluon. On the other hand, in the large energy (small-$x$) limit, the characteristic scale $\mu$ of the hard subprocess of parton scattering is much less than $\sqrt{s}$, but greater than the $\Lambda_{\mathrm{QCD}}$ parameter. In this limit, the effects of the finite transverse momenta of the incoming partons become important, and the factorization must be generalized, implying that the cross sections are now $k_T$-factorized into an off-shell partonic cross section and a $k_T$-unintegrated parton density function $\mathcal{F}(x, k_T)$, characterizing the $k_T$-factorization approach. The function $\mathcal{F}$ is obtained as a solution of the evolution equation associated to the dynamics that governs QCD at high energies. Several authors have considered the $k_T$-factorization approach in order to analyze some observables and they have obtained a better description of these quantities than the one obtained with the collinear approach. However, the current situation is still not satisfactory, due to the large uncertainty associated to the lack of a complete knowledge of the unintegrated gluon distribution. In particular, at high energies the non-linear QCD effects associated to the gluon saturation are expected to contribute significantly and this leads to the breakdown of the twist expansion and of the factorization schemes.

Gluon saturation effects can be naturally described in the color dipole formalism. At high energies color dipoles with a defined transverse separation are eigenstates of the interaction. The main quantity in this formalism is the dipole–target cross section, which is universal and determined by QCD dynamics at high energies. In particular, it provides a unified description of inclusive and diffractive observables in $ep$ processes as well as for in Drell–Yan, prompt photon and heavy quark production in hadron–hadron collisions. Furthermore, an important advantage of this formalism is that it is very simple to include nuclear effects (see below).

In the color dipole formalism the total cross section for the process $h_1 h_2 \to Q\bar{Q}X$, where $h_i = p$ or $A$, is given by [19,20]:

$$\sigma_{tot}\big(h_1 h_2 \to \{Q\bar{Q}\}X\big) = 2 \int_0^{-\ln(2m_Q/\sqrt{s})} dy\, x_1 G_{h_1}(x_1, \mu_F)\sigma\big(Gh_2 \to \{Q\bar{Q}\}X\big) \tag{1}$$

where $x_1 G_{h_1}(x_1, \mu_F)$ is the projectile gluon distribution, the cross section $\sigma(Gh_2 \to \{Q\bar{Q}\}X)$ describes the heavy quark production in the gluon–target interaction, $y$ is the rapidity of the pair and $\mu_F$ is the factorization scale, which we assume to be given by $\mu_F = 2m_Q$. The proton gluon distribution will be taken from the set of parton densities GRV98 [26], but similar predictions are obtained using e.g. the CTEQ6L parametrization. Eq. (1) can be easily interpreted in the target rest frame, where heavy quark production looks like pair creation in the target color field. For a short time, a gluon $G$ from the projectile hadron can develop a fluctuation which contains a heavy quark pair ($Q\bar{Q}$). The interaction with the color field of the target may then release these heavy quarks. This mechanism corresponds to the gluon–gluon fusion mechanism of heavy quark production in the leading order (LO) parton model. The dipole formulation is therefore applicable only at low $x$, where the gluon density of the target is much larger than all quark densities. This condition is fulfilled for the charm and bottom production at the CERN-LHC.

The cross section for the process $G + h_2 \to Q\bar{Q}X$ is given by:

$$\sigma\big(Gh_2 \to \{Q\bar{Q}\}X\big) = \int_0^1 d\alpha \int d^2\rho \left|\Psi_{G\to Q\bar{Q}}(\alpha,\rho)\right|^2 \sigma^{h_2}_{q\bar{q}G}(\alpha,\rho) \tag{2}$$

where $\sigma^{h_2}_{q\bar{q}G}$ is the scattering cross section of a color neutral quark–antiquark–gluon system on the hadron target $h_2$ [19–22]:

$$\sigma^{h_2}_{q\bar{q}G}(\alpha,\rho) = \frac{9}{8}\big[\sigma_{q\bar{q}}(\alpha\rho) + \sigma_{q\bar{q}}(\bar{\alpha}\rho)\big] - \frac{1}{8}\sigma_{q\bar{q}}(\rho). \tag{3}$$

The quantity $\sigma_{q\bar{q}}$ is the scattering cross section of a color neutral quark–antiquark pair with separation radius $\rho$ on the target and $\alpha$ ($\bar{\alpha} = 1-\alpha$) is the fractional momentum of quark (antiquark). The light-cone (LC) wave function of the transition $G \to Q\bar{Q}$ can be calculated perturbatively, with the squared wave function given by:

$$\left|\Psi_{G\to Q\bar{Q}}(\alpha,\rho)\right|^2 = \frac{\alpha_s(\mu_R)}{(2\pi)^2}\big\{m_Q^2 K_0^2(m_Q\rho) + \big[\alpha^2+\bar{\alpha}^2\big]m_Q^2 K_1^2(m_Q\rho)\big\} \tag{4}$$

where $\alpha_s(\mu_R)$ is the strong coupling constant, which is computed at a renormalization scale $\mu_R$, which we assume to be equal to quark mass, and it is given by:

$$\alpha_s(\mu_R) = \frac{4\pi}{(11-\frac{2}{3}N_f)\ln(\frac{\mu_R^2}{(200\ \mathrm{MeV})^2})}. \tag{5}$$

Another observable of interest is the rapidity distribution, which in the dipole formalism is expressed as:

$$\frac{d\sigma(h_1h_2 \to \{Q\bar{Q}\}X)}{dy} = x_1 G^{h_1}\big(x_1,\mu_F^2\big)\sigma\big(Gh_2 \to \{Q\bar{Q}\}X\big). \tag{6}$$

Before discussing the QCD dynamics at high energies in the next section, some comments are in order. First, in the dipole formalism we work in a mixed representation, where the longitudinal direction is treated in momentum space, while the transverse directions are described in the coordinate space representation. Second, in Ref. [22] the equivalence between this approach and the gluon–gluon fusion mechanism of the conventional collinear factorization at leading order and twist has been demonstrated. In particular, the dipole predictions are similar to those obtained using the next-to-leading order parton model calculation. However, it is important to emphasize that Eq. (1) resums higher-twist corrections beyond the traditional factorization schemes.

## 3. QCD dynamics

The main ingredient of the dipole formalism is the dipole–target cross section $\sigma_{q\bar{q}}$ which is determined by the QCD dynamics. At leading logarithmic approximation it is directly related to the target gluon distribution $xG_{h_2}$ as follows [27]:

$$\sigma_{q\bar{q}}\big(x,\rho^2\big) = \frac{\pi^2}{3}\rho^2\alpha_s x G_{h_2}\big(x,10/\rho^2\big), \tag{7}$$

which satisfies the property known as color transparency, i.e. $\sigma_{q\bar{q}}$ vanishes $\propto \rho^2$ at small separations. If we assume that $xG_{h_2}$ is a solution of the DGLAP evolution equations, the use of

this expression as input in our calculations implies that we are disregarding non-linear QCD effects, associated to the high gluon density present at small-$x$ (large energies). In what follows we assume that the resulting predictions correspond to the linear QCD dynamics and denote them by CT in the plots. When the target is a proton we assume that the gluon distribution is given by the GRV98 parametrization [26]. If the target is a nucleus we will assume that $xG_A(x, Q^2) = A.R_g(x, Q^2).xG_N(x, Q^2)$ with $xG_N$ being the gluon distribution in the proton and $R_g$ given by the EPS09 [28] or DS [29] parametrizations for the nuclear effects. In both cases we are disregarding multiple scatterings of the dipole with the nuclei and are assuming that the dipole interacts incoherently with the target. Expression (7) was recently used in [30] to give the linear physics predictions for heavy quark production in $eA$ collisions.

The results from HERA, RHIC and more recently from the LHC suggest that $ep$ and hadron–hadron interactions at high energies probe QCD in the non-linear regime of high parton densities, where the growth of parton distributions should saturate, possibly forming a Color Glass Condensate [31]. This formalism implies that the dipole–target cross section $\sigma_{q\bar{q}}$ is given in terms of the dipole–target forward scattering amplitude $\mathcal{N}(x, \rho, \boldsymbol{b})$, which encodes all the information about the hadronic scattering, and thus about the non-linear and quantum effects in the hadron wave function. It reads:

$$\sigma_{q\bar{q}}(x, \rho) = 2 \int d^2\boldsymbol{b}\, \mathcal{N}(x, \rho, \boldsymbol{b}). \tag{8}$$

It is useful to assume that the impact parameter dependence of $\mathcal{N}$ can be factorized as $\mathcal{N}(x, \rho, \boldsymbol{b}) = \mathcal{N}(x, \rho)S(\boldsymbol{b})$, so that $\sigma_{q\bar{q}}(x, \rho) = \sigma_0\mathcal{N}(x, \rho)$, with $\sigma_0$ being a free parameter related to the non-perturbative QCD physics. The Balitsky–JIMWLK hierarchy [31] describes the energy evolution of the dipole–target scattering amplitude $\mathcal{N}(x, \rho)$. In the mean field approximation, the first equation of this hierarchy decouples and boils down to the Balitsky–Kovchegov (BK) equation [32,33].

In the last years the next-to-leading order corrections to the BK equation were calculated [34–36] through the resummation of $\alpha_s N_f$ contributions to all orders, where $N_f$ is the number of flavors. Such calculation allows one to estimate the soft gluon emission and running coupling corrections to the evolution kernel. The authors have found out that the dominant contributions come from the running coupling corrections, which allow us to determine the scale of the running coupling in the kernel. The solution of the improved BK equation was studied in detail in Refs. [35,37]. The running of the coupling reduces the speed of the evolution to values compatible with experimental data, with the geometric scaling regime being reached only at ultra-high energies. In [38] a global analysis of the small $x$ data for the proton structure function using the improved BK equation was performed (see also Ref. [39]). In contrast to the BK equation at leading logarithmic $\alpha_s \ln(1/x)$ approximation, which fails to describe the HERA data, the inclusion of running coupling effects in the evolution renders the BK equation compatible with them (see also [40–42]). In what follows we consider the BK predictions for $\mathcal{N}(x, \rho)$ obtained using the GBW [43] initial condition.

The dipole–target cross section can also be calculated considering phenomenological parametrizations for $\mathcal{N}(x, \rho)$ based on saturation physics, which provide an economical description of a wide range of data with a few parameters. Several models for the forward dipole cross section have been used in the literature in order to fit the HERA and RHIC data. In general, the dipole scattering amplitude is modeled in the coordinate space in terms of a simple Glauber-like formula as follows

$$\mathcal{N}(x,\rho) = 1 - \exp\left[-\frac{1}{4}\left(\rho^2 Q_s^2\right)^{\gamma(x,\rho^2)}\right], \tag{9}$$

where $\gamma$ is the anomalous dimension of the target gluon distribution. The main difference among the distinct phenomenological models comes from the predicted behavior for the anomalous dimension, which determines the transition from the non-linear to the extended geometric scaling regimes, as well as from the extended geometric scaling to the DGLAP regime (see e.g. [18]). The current models in the literature consider the general form $\gamma = \gamma_s + \Delta\gamma$, where $\gamma_s$ is the anomalous dimension at the saturation scale and $\Delta\gamma$ mimics the onset of the geometric scaling region and DGLAP regime. In what follows we compare the rcBK [38] predictions with those of the GBW model [43], which assumes $\gamma(x,\rho^2) = 1$.

In order to estimate heavy quark production in $pA$ collisions we will use the fact that color dipoles are eigenstates of the interaction and therefore the $q\bar{q}G$–nucleus interaction can be expressed in terms of the cross section on a nucleon target using the Glauber–Mueller formalism:

$$\sigma^A_{q\bar{q}G}(x,\rho) = 2\int d^2\boldsymbol{b}\left\{1 - \exp\left[-\frac{1}{2}\sigma^p_{q\bar{q}G}\left(x,\rho^2\right)T_A(\boldsymbol{b})\right]\right\}, \tag{10}$$

where $\sigma^p_{q\bar{q}G}$ is given by Eq. (3) and $T_A(\boldsymbol{b})$ is the nuclear profile function, which is obtained from a 3-parameter Fermi distribution for the nuclear density normalized to $A$. The above equation sums up all the multiple elastic rescattering diagrams of the $q\bar{q}G$ system and is justified for large coherence length, where the transverse separation $\rho$ of partons in the multiparton Fock state of the projectile becomes a conserved quantity, i.e. the size of the dipole becomes eigenvalue of the scattering matrix. In the next section we will estimate Eq. (10) using as input the rcBK and GBW models for the dipole–proton cross section. Moreover, we will compare these predictions with those obtained using the CT model generalized to the nuclear case.

Recently a comprehensive study of the $k_T$-factorization at high energies was performed in Refs. [44,45], which have addressed dijet production in various processes in the small-$x$ limit and an effective factorization for hard processes in systems with dilute probes scattering on dense targets was established. In particular, the authors have analyzed in detail the $G \to q\bar{q}$ channel using the Color Glass Condensate formalism (see Section IV.B.2 in [45]), which allows us to obtain an expression for the $\sigma^A_{q\bar{q}G}$ total cross section given by:

$$\begin{aligned}\sigma^A_{q\bar{q}G}(\alpha,\rho) = \int d^2\boldsymbol{b}\Bigg\{&\frac{9}{8}\left[1 - \exp\left[\left(-\sigma_{q\bar{q}}(\alpha\rho) - \sigma_{q\bar{q}}(\bar{\alpha}\rho)\right)T_A(\boldsymbol{b})\right]\right] \\ &- \frac{1}{8}\left[1 - \exp\left(-\sigma_{q\bar{q}}(\rho)T_A(\boldsymbol{b})\right)\right]\Bigg\},\end{aligned} \tag{11}$$

which reduces to Eq. (3) in the dilute limit. In what follows we calculate the above expression using $\sigma_{q\bar{q}}$ given by the GBW dipole–proton model and we will denote by CGC the predictions obtained using Eq. (11) as input in our calculations of the heavy quark production cross sections.

Another issue that we will address is the asymmetry in heavy quark production in $pA$ collisions when we use the color dipole formalism. Our treatment of the interaction is not symmetric under the projectile–target exchange. In particular, $pA$ and $Ap$ processes allow us to study different physical effects. While $pA$ collisions allow to study non-linear effects in the dipole–nucleus interaction, the study of $Ap$ collisions probes the nuclear effects in the projectile gluon distribution. The rapidity distribution in the latter case is given by:

$$\frac{d\sigma(Ap \to \{Q\bar{Q}\}X)}{dy} = x_1 G^A\left(x_1,\mu_F^2\right)\sigma\left(Gp \to \{Q\bar{Q}\}X\right). \tag{12}$$

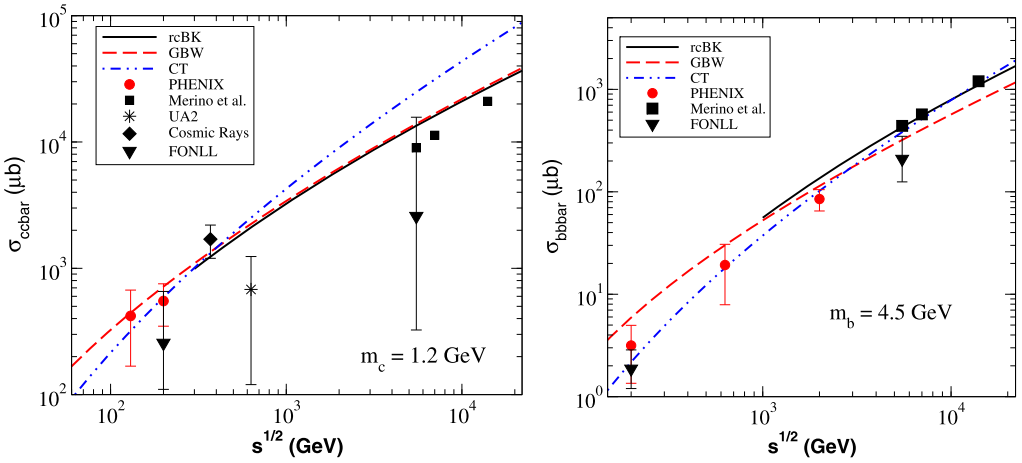


Fig. 1. (Color online.) Total charm (left) and bottom (right) production cross sections in proton–proton collisions as a function of the c.m.s. energy ($\sqrt{s}$). Data points from PHENIX [15,16] (circles), from UA2 [47] (down triangles) and from cosmic ray [48] (diamonds). Theoretical results obtained with $k_T$ factorization [49] (squares) and with FONLL [50] (up triangles).

As it can be seen, this process can be used to constrain the magnitude the shadowing and antishadowing effects, which is still an open question (for a similar discussion in the Drell–Yan process see Ref. [46]). It is important to emphasize that the factorization assumed in Eq. (12), denoted usually hybrid $k_T$-factorization, is well justified for collisions of a dilute projectile in a dense target [45]. Consequently, its use in $Ap$ collisions should be considered exploratory. However, as at high energies and backward rapidities the saturation scale in the proton is large and we are probing the nucleus at large-$x$, we believe that our estimates can be considered as a reasonable first approximation for the cross sections.

## 4. Results

In Fig. 1 we show the predictions of the color dipole formalism for the total heavy quark production cross sections in proton–proton collisions as a function of the c.m.s. energy ($\sqrt{s}$) using as input the CT, GBW and rcBK dipole cross sections. The left (right) panels show charm (bottom) cross sections. As the rcBK dipole cross section can be calculated only for small $x$ ($\leqslant 10^{-2}$), we are not able to obtain results for heavy quark production at the lowest energies. We compare our results with the experimental data obtained by the PHENIX Collaboration [15,16] (circles), by the UA2 Collaboration [47] (up triangles) and with data extracted from cosmic ray measurements [48] (diamonds). We also show the theoretical results obtained with the $k_T$ factorization scheme [49] (squares) and with FONLL [50] (down triangles). Our results were obtained assuming $m_c = 1.2$ GeV and $m_b = 4.5$ GeV. In the case of the GBW and rcBK predictions these values of mass allow us to describe satisfactorily the experimental data without the inclusion of a $K$-factor to fit the normalization. However, in the CT case it is necessary to multiply the prediction by $K = 0.4$ in order to describe the experimental data. This factor becomes equal to one if the mass is increased, since (as in other approaches) there is a strong dependence of the results on the choice of the heavy quark mass. This strong dependence is observed in Fig. 2 for the CT input ($K = 1$ in this figure) and similar results are obtained using the GBW and rcBK inputs.

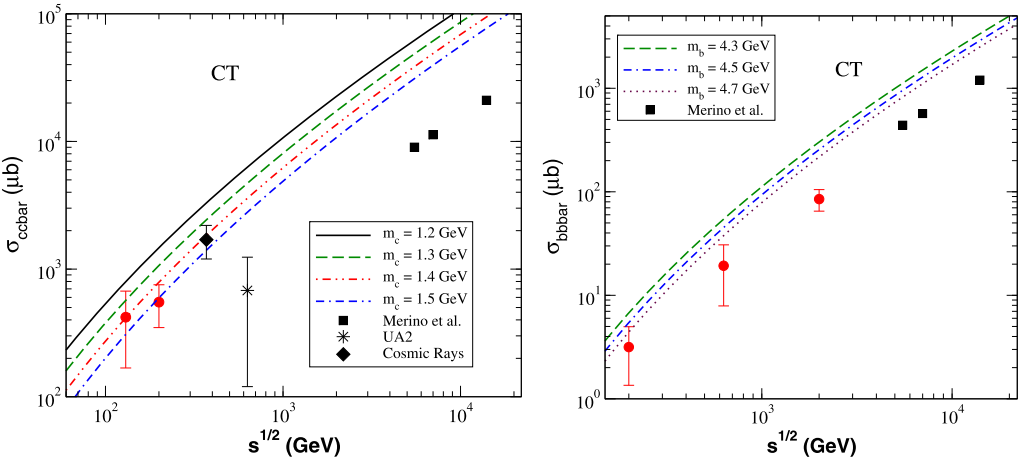


Fig. 2. (Color online.) Dependence on the mass of the total charm (left) and bottom (right) production cross sections in proton–proton collisions as a function of the c.m.s. energy ($\sqrt{s}$) obtained with the GBW dipole cross section.

In what follows we will assume the same values for the heavy quark masses in all calculations. Beyond the mass dependence, the heavy quark cross sections are also strongly dependent on the renormalization and factorization scales. We postpone the discussion about this dependence for a future work and assume $\mu_R = m_Q$.

From Fig. 1 we can see that in the case of charm production the rcBK and GBW predictions are very similar at high energies, while the CT one predicts a stronger growth of the cross section with the energy. This difference comes from saturation effects which are expected to significantly contribute in the kinematical region in which $Q_s^2 > m_Q^2$. On the other hand, in the case of bottom production the rcBK and CT predictions are similar and larger than the GBW one. This behavior can be attributed to the description of the linear regime which is different in the rcBK and GBW dipole–proton cross sections. In particular, the numerical solutions of the BK equation tend to reach later the unitarity limit [40]. This can be understood looking carefully at the integrand of (2), which is the product of the wave functions, containing information about the masses, and the dipole cross section. As a function of the dipole size, $\rho$, the difference between GBW and rcBK is mostly in the low to intermediate $\rho$ region, where the GBW is always below the rcBK dipole cross section. At large $\rho$ the two cross sections are close to each other. The squared wave function, i.e., $(\Psi^*\Psi)$ given by (4) has peaks at different locations in $\rho$. The $c\bar{c}$ is a larger state and its wave function peaks at much larger values of $\rho$ than the $b\bar{b}$ wave function. In this way it gives a stronger weight to larger $\rho$ where the differences between GBW and rcBK are smaller. A similar effect was also observed in a previous calculation with the rcBK dipole cross section. The exclusive vector meson production cross sections change when we change the dipole cross section. One of the conclusions of [51] was that the difference between results with rcBK and bCGC becomes more pronounced for heavier mesons. Our results suggest that with the total cross section alone we are not able to discriminate between the different dynamics contained in the dipole–proton cross sections. On the other hand it is reassuring to observe the compatibility of our results both with data and with other theoretical estimates.

We address now heavy quark production in $pA$ collisions. In the absence of nuclear effects, the heavy quark cross section would simply scale with the atomic number. Therefore departures from the $A$ scaling provide information about nuclear effects. Here we consider the influence of

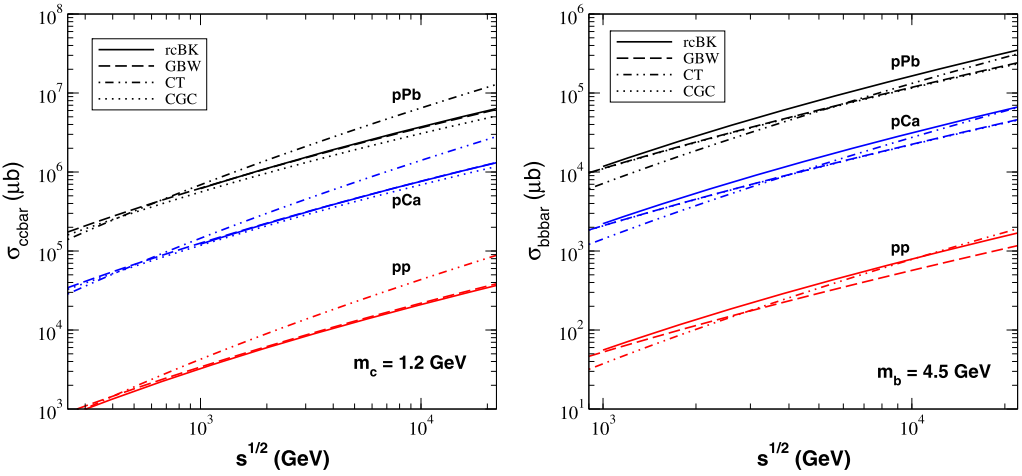


Fig. 3. (Color online.) Target mass dependence of the total charm (left) and bottom (right) production cross sections in $p$Pb and $p$Ca collisions as a function of the c.m.s. energy ($\sqrt{s}$). For comparison the $pp$ predictions are also show.

saturation and shadowing. Both effects are expected to strongly affect heavy quark production at high energies but the relation between them is not clear. We assume two extreme scenarios: the coherent, based on the non-linear dynamics, and the incoherent one, based on the linear DGLAP dynamics. Our goal is to verify if it is possible to discriminate these scenarios.

In Fig. 3 we present our predictions for the heavy quark production in $pA$ collisions considering $A =$ Ca and Pb. For comparison the $pp$ predictions are also shown. In the nuclear case and charm production, the GBW and rcBK predictions are very similar, as already observed in the proton case. The difference between these predictions and those from CT increases with the atomic number. This fact can be attributed to the growth of the contribution of saturation effects. It is important to remember that the nuclear saturation scale is expected to increase with $A^{\frac{1}{3}}$, which implies that the kinematical regime where $Q_s^2 > m_Q^2$ is enlarged in $pA$ collisions at high energies. Moreover, the difference between the coherent prediction, obtained using Eq. (10), and the incoherent one, obtained using the CT model, can be larger if the shadowing effects are disregarded in $xG_A$. The CT predictions for the nuclear case in Fig. 3 were obtained using the EPS09 [28] parametrization of the nuclear effects, which predicts a large shadowing effect at small-$x$, implying a strong reduction of the magnitude of the charm cross section. In the bottom case the magnitude of saturation and shadowing effects is smaller and therefore the difference between the CT and rcBK predictions is also smaller. As in the proton case, the GBW model predicts a distinct behavior in the bottom case, that implies a mild growth of the cross section with the energy. When the CGC model [Eq. (11)] is used as input, the resulting predictions are similar to those from the Glauber–Mueller model, with a mild energy dependence in the charm case. In the bottom case the CGC and GBW predictions are identical, which is directly associated to the dominance of small pair separations.

In Fig. 4 we present our predictions for the charm (left panel) and bottom (right panel) rapidity distributions in $pp$, $p$Ca and $p$Pb collisions. For comparison we use the same value of center-of-mass energy: $\sqrt{s} = 7$ TeV. In the charm case, as already observed for the total cross section, the rcBK, GBW and CGC predictions are very similar and smaller than the CT one, with the

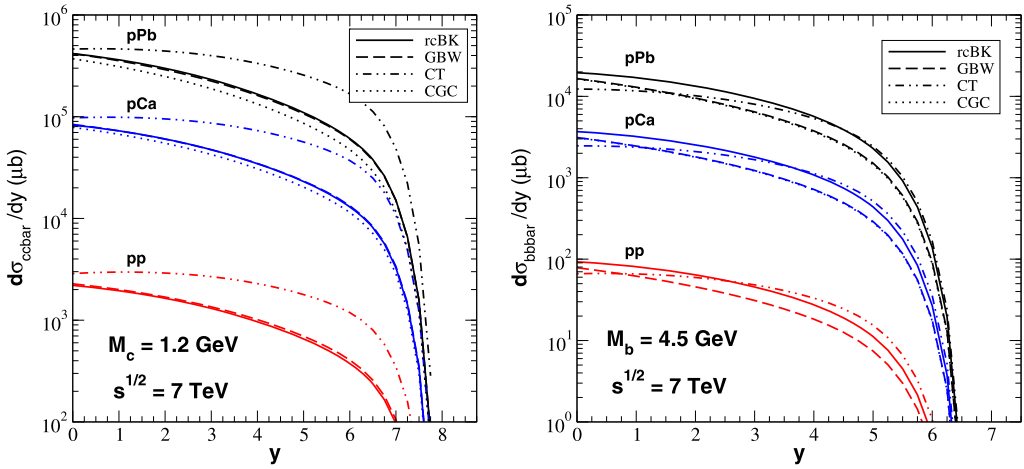


Fig. 4. (Color online.) Rapidity distributions for charm (left panel) and bottom (right panel) production in $pp$, $p$Ca and $p$Pb collisions at $\sqrt{s} = 7$ TeV.

difference increasing with the rapidity. On the other hand, in the bottom case, the rcBK and CT predictions are larger than the GBW and CGC one.

In order to estimate more precisely the difference between the predictions and the magnitude of the effects, in Figs. 5 and 6 we present our predictions for the normalized ratio between the rapidity distributions for charm and bottom production, respectively. In these figures we choose $\sqrt{s} = 8.8$ TeV, which is the expected center-of-mass energy for $pA$ runs at LHC. As expected the ratio diminishes at larger $y$ and $A$ and smaller heavy quark mass. In the charm case, the ratio is smaller than one for all dipole–target models. While the rcBK model predicts the largest value for the ratio, the CT one predicts smaller values than the Glauber–Mueller predictions (rcBK and GBW). This behavior can be related to the magnitude of the shadowing effects present in the EPS09 nuclear gluon distribution. In contrast, the CGC model predicts the smallest values for the ratio. The large difference between the GBW and CGC predictions implies that the study of the ratio can be useful to determinate the correct model to describe the $\sigma^A_{q\bar{q}G}$ cross section. In the bottom case, the rcBK, GBW and CGC models predict values about one while the CT one predicts that the ratio is strongly reduced. Therefore, the behavior of the ratio is strongly dependent on the model used to describe the dipole–nucleus interaction.

As discussed in the previous section, the color dipole formalism for heavy quark production in proton–nucleus collisions is asymmetric under projectile–target exchange. In what follows we estimate the rapidity distribution for charm and bottom production at $\sqrt{s} = 8.8$ TeV using Eq. (12) and assuming that the gluon distribution $xG_A$ is given by a parametrization of the nuclear effects and that the dipole–proton cross section is given by the rcBK prediction. In Fig. 7 we present our predictions considering the EPS09 [28] and nDS [29] parametrizations of the nuclear effects. For comparison we also present the prediction obtained disregarding nuclear effects. The region of negative rapidity probes small values of $x$ in the nuclear gluon distribution $[x_1 = (m_Q/\sqrt{s})e^{+y}]$ and consequently the magnitude of shadowing effects. At LHC energies, this is also valid at midrapidity. In contrast, at large $y$ we are probing antishadowing. It can be explicitly observed by the coincidence between the prediction obtained disregarding the nuclear effects (denoted No Shad in the figure) and the nDS prediction. One of the basic features of this parametrization is that antishadowing is not present in the gluon distribution. Another feature is

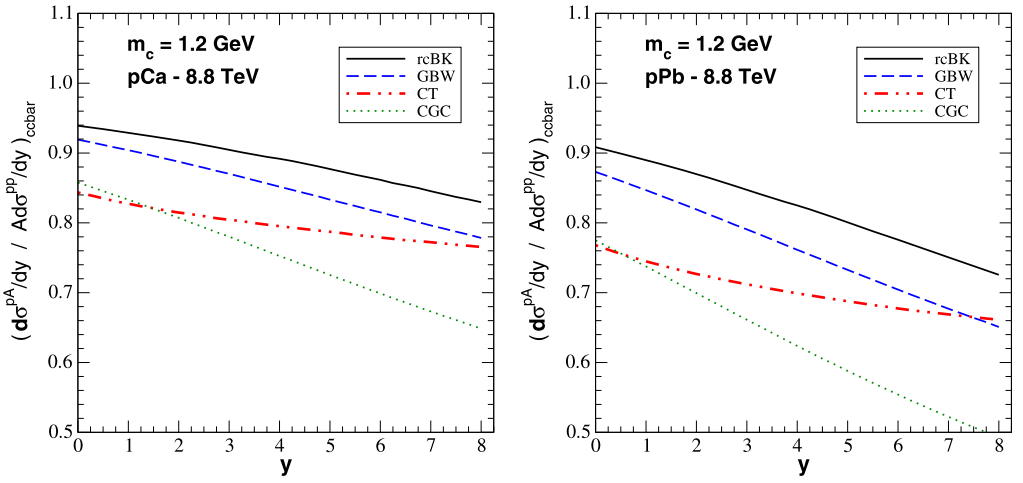


Fig. 5. (Color online.) Rapidity dependence of the normalized ratio between charm rapidity distributions in $p$Ca (left) and $p$Pb (right) collisions at $\sqrt{s} = 8.8$ TeV.

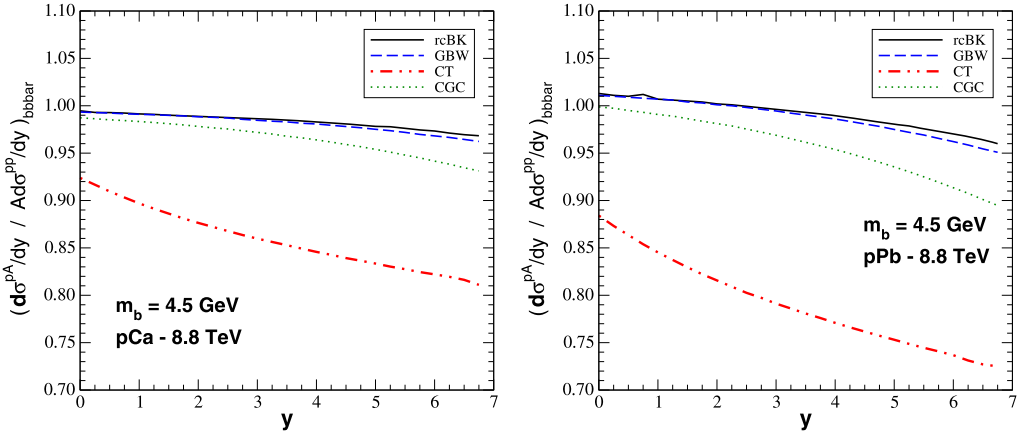


Fig. 6. (Color online.) Rapidity dependence of the normalized ratio between bottom rapidity distributions in $p$Ca (left) and $p$Pb (right) collisions at $\sqrt{s} = 8.8$ TeV.

the small magnitude of shadowing. As observed the nDS and No Shad predictions are similar for the bottom production, the nDS one being a little smaller in the case of charm. In contrast, EPS09 predicts a strong reduction at $y < 4.2(2.7)$ and charm (bottom) production. This behavior is more easily observed if we calculate the ratio between the rapidity distributions calculated using the EPS09 or nDS and disregarding the nuclear effects. The rapidity dependence of this ratio is show in Fig. 8. This ratio is approximately one in the nDS case and present a strong dependence in the EPS09 case.

## 5. Summary

The description of heavy quark production is one the most important testing grounds for perturbative QCD. Currently, there are several approaches which satisfactorily describe the available

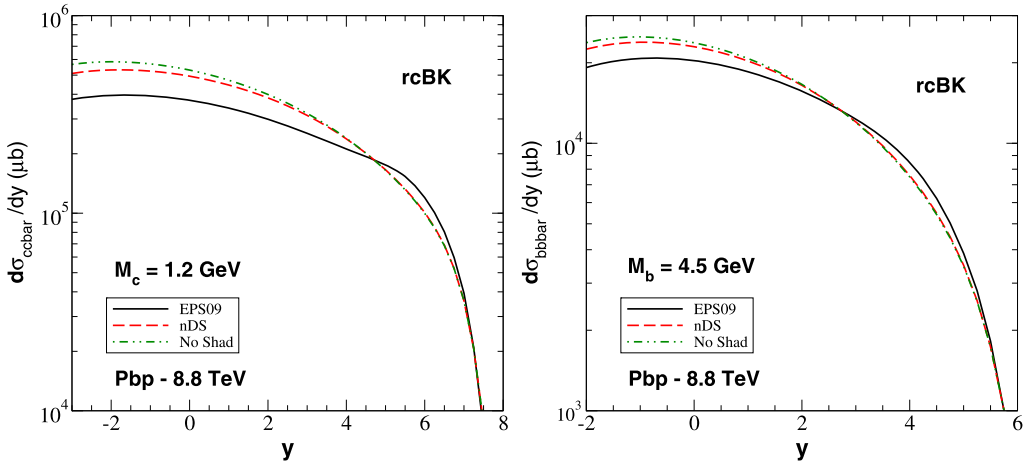


Fig. 7. (Color online.) Rapidity distributions of charm (left) and bottom (right) produced in $Ap$ collisions at $\sqrt{s} = 8.8$ TeV.

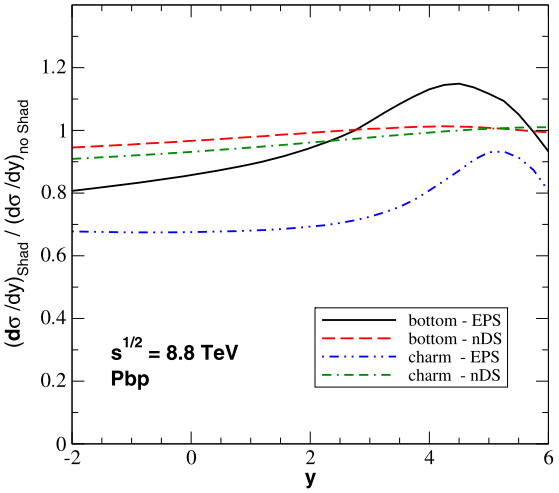


Fig. 8. (Color online.) Rapidity dependence of the ratio between rapidity distributions with and without nuclear effects.

experimental data. However, it is still an open question whether standard pQCD works well at higher energies and in nuclear collisions. In this regime, the traditional factorization schemes based on a twist expansion, are expected to breakdown due to the presence of saturation effects associated to the high parton density and all twists should be resummed. In this paper we have computed heavy quark production in $pp$ and $pA$ collisions considering the color dipole formalism, which allows to include saturation effects (which are expected to be present at high energies and large nuclei). In particular, we analyze the energy dependence of the total cross section and the behavior of the rapidity distribution at fixed energy considering two distinct approaches to treat the dipole–target interaction. One based on the non-linear QCD dynamics and another associated to the linear QCD dynamics. Our results shown that the influence of the saturation or shadowing effects is different for charm and bottom production and therefore the simultaneous

analyses of the associated observables can be useful to discriminate the dynamics. Furthermore, we analyze $Ap$ collisions as a probe of shadowing effects in nuclear gluon densities and demonstrate that the study of rapidity distributions should allow to constrain their magnitude.

## Acknowledgements

This work was partially financed by the Brazilian funding agencies CNPq, CAPES and FAPERGS.

## References

[1] P. Nason, S. Dawson, R.K. Ellis, Nucl. Phys. B 303 (1988) 607.
[2] G. Altarelli, M. Diemoz, G. Martinelli, P. Nason, Nucl. Phys. B 308 (1988) 724.
[3] P. Nason, S. Dawson, R.K. Ellis, Nucl. Phys. B 327 (1989) 49;
P. Nason, S. Dawson, R.K. Ellis, Nucl. Phys. B 335 (1990) 260, Erratum.
[4] W. Beenakker, H. Kuijf, W.L. van Neerven, J. Smith, Phys. Rev. D 40 (1989) 54.
[5] M. Cacciari, M. Greco, P. Nason, JHEP 9805 (1998) 007.
[6] S. Catani, M. Ciafaloni, F. Hautmann, Phys. Lett. B 242 (1990) 97.
[7] S. Catani, M. Ciafaloni, F. Hautmann, Nucl. Phys. B 366 (1991) 135.
[8] J.C. Collins, R.K. Ellis, Nucl. Phys. B 360 (1991) 3.
[9] G. Marchesini, B.R. Webber, Nucl. Phys. B 310 (1988) 461;
G. Marchesini, B.R. Webber, Nucl. Phys. B 386 (1992) 215.
[10] P. Hagler, R. Kirschner, A. Schafer, L. Szymanowski, O. Teryaev, Phys. Rev. D 62 (2000) 071502.
[11] L.V. Gribov, E.M. Levin, M.G. Ryskin, Phys. Rep. 100 (1983) 1.
[12] E.M. Levin, M.G. Ryskin, Phys. Rep. 189 (1990) 267.
[13] Yu.M. Shabelski, A.G. Shuvaev, Phys. Atom. Nucl. 69 (2006) 314.
[14] H. Jung, M. Kraemer, A.V. Lipatov, N.P. Zotov, arXiv:1105.5071;
H. Jung, M. Kraemer, A.V. Lipatov, N.P. Zotov, arXiv:1107.4328;
H. Jung, M. Kraemer, A.V. Lipatov, N.P. Zotov, JHEP 1101 (2011) 085.
[15] K. Adcox, et al., PHENIX Collaboration, Phys. Rev. Lett. 88 (2002) 192303.
[16] A. Adare, et al., PHENIX Collaboration, Phys. Rev. Lett. 97 (2006) 252002.
[17] J. Bielcik, STAR Collaboration, arXiv:nucl-ex/0606010.
[18] F. Gelis, E. Iancu, J. Jalilian-Marian, R. Venugopalan, Annu. Rev. Nucl. Part. Sci. 60 (2010) 463.
[19] N.N. Nikolaev, G. Piller, B.G. Zakharov, J. Exp. Theor. Phys. 81 (1995) 851, Zh. Eksp. Teor. Fiz. 108 (1995) 1554.
[20] N.N. Nikolaev, G. Piller, B.G. Zakharov, Z. Phys. A 354 (1996) 99.
[21] B.Z. Kopeliovich, A.V. Tarasov, Nucl. Phys. A 710 (2002) 180.
[22] J. Raufeisen, J.C. Peng, Phys. Rev. D 67 (2003) 054008.
[23] K. Tuchin, Nucl. Phys. A 798 (2008) 61.
[24] Y.V. Kovchegov, K. Tuchin, Phys. Rev. D 74 (2006) 054014.
[25] K. Tuchin, Phys. Lett. B 593 (2004) 66.
[26] M. Glück, E. Reya, A. Vogt, Eur. Phys. J. C 5 (1998) 461.
[27] N.N. Nikolaev, B.G. Zakharov, Phys. Lett. B 332 (1994) 184;
N.N. Nikolaev, B.G. Zakharov, Z. Phys. C 64 (1994) 631.
[28] K.J. Eskola, H. Paukkunen, C.A. Salgado, JHEP 0904 (2009) 065.
[29] D. de Florian, R. Sassot, Phys. Rev. D 69 (2004) 074028.
[30] V.P. Goncalves, M.S. Kugeratski, F.S. Navarra, Phys. Rev. C 81 (2010) 065209.
[31] J. Jalilian-Marian, A. Kovner, L. McLerran, H. Weigert, Phys. Rev. D 55 (1997) 5414;
J. Jalilian-Marian, A. Kovner, H. Weigert, Phys. Rev. D 59 (1999) 014014;
J. Jalilian-Marian, A. Kovner, H. Weigert, Phys. Rev. D 59 (1999) 014015;
J. Jalilian-Marian, A. Kovner, H. Weigert, Phys. Rev. D 59 (1999) 034007;
A. Kovner, J.G. Milhano, H. Weigert, Phys. Rev. D 62 (2000) 114005;
H. Weigert, Nucl. Phys. A 703 (2002) 823;
E. Iancu, A. Leonidov, L. McLerran, Nucl. Phys. A 692 (2001) 583;
E. Ferreiro, E. Iancu, A. Leonidov, L. McLerran, Nucl. Phys. A 701 (2002) 489.

[32] I.I. Balitsky, Nucl. Phys. B 463 (1996) 99;
I.I. Balitsky, Phys. Rev. Lett. 81 (1998) 2024;
I.I. Balitsky, Phys. Rev. D 60 (1999) 014020;
I.I. Balitsky, Phys. Lett. B 518 (2001) 235;
I.I. Balitsky, A.V. Belitsky, Nucl. Phys. B 629 (2002) 290.
[33] Y.V. Kovchegov, Phys. Rev. D 60 (1999) 034008;
Y.V. Kovchegov, Phys. Rev. D 61 (2000) 074018.
[34] Y.V. Kovchegov, H. Weigert, Nucl. Phys. A 784 (2007) 188;
Y.V. Kovchegov, H. Weigert, Nucl. Phys. A 789 (2007) 260;
Y.V. Kovchegov, J. Kuokkanen, K. Rummukainen, H. Weigert, Nucl. Phys. A 823 (2009) 47.
[35] J.L. Albacete, Y.V. Kovchegov, Phys. Rev. D 75 (2007) 125021.
[36] I. Balitsky, Phys. Rev. D 75 (2007) 014001;
I. Balitsky, G.A. Chirilli, Phys. Rev. D 77 (2008) 014019.
[37] J.L. Albacete, Phys. Rev. Lett. 99 (2007) 262301.
[38] J.L. Albacete, N. Armesto, J.G. Milhano, C.A. Salgado, Phys. Rev. D 80 (2009) 034031.
[39] H. Weigert, J. Kuokkanen, K. Rummukainen, AIP Conf. Proc. 1105 (2009) 394.
[40] M.A. Betemps, V.P. Goncalves, J.T. de Santana Amaral, Eur. Phys. J. C 66 (2010) 137.
[41] J.L. Albacete, C. Marquet, Phys. Lett. B 687 (2010) 174.
[42] V.P. Goncalves, M.V.T. Machado, A.R. Meneses, Eur. Phys. J. C 68 (2010) 133.
[43] K. Golec-Biernat, M. Wusthoff, Phys. Rev. D 59 (1999) 014017;
K. Golec-Biernat, M. Wusthoff, Phys. Rev. D 60 (1999) 114023.
[44] F. Dominguez, B.W. Xiao, F. Yuan, Phys. Rev. Lett. 106 (2011) 022301.
[45] F. Dominguez, C. Marquet, B.W. Xiao, F. Yuan, Phys. Rev. D 83 (2011) 105005.
[46] M.A. Betemps, M.B.G. Ducati, E.G. de Oliveira, Phys. Rev. D 74 (2006) 094010.
[47] O. Botner, et al., UA2 Collaboration, Phys. Lett. B 236 (1990) 488.
[48] Z. Xu, J. Phys. G 32 (2006) S309, nucl-ex/0607015.
[49] C. Merino, C. Pajares, M.M. Ryzhinskiy, Yu.M. Shabelski, A.G. Shuvaev, Phys. Atom. Nucl. 73 (2010) 1781;
C. Merino, C. Pajares, M.M. Ryzhinskiy, Yu.M. Shabelski, A.G. Shuvaev, Phys. Atom. Nucl. 74 (2011) 173, Erratum.
[50] R. Vogt, Eur. Phys. J. C 61 (2009) 793.
[51] E.R. Cazaroto, F. Carvalho, V.P. Gonçalves, M.S. Kugeratski, F.S. Navarra, Phys. Lett. B 696 (2011) 473.